Transform Domain Based Hybrid Element Formulations for Transient Electromagnetic Field Computations

P. Jose[1], R.Kanapady[2] and K.K.Tamma[3]

Abstract: In this article, a novel hybrid finite element and Laplace transform formulation is presented for the computations of transient electromagnetic fields. The formulation is first based on application of Laplace transform technique for the pertinent differential equations, namely the Maxwell's equation in the non-integral form with subsequently, employing the Galerkin finite element formulations on the transformed equations to maintain the modeling versatility of complex geometries and numerical features for computational analysis. In addition, in conjunction with the above, proper scaling of the field quantities is applied to improve the condition of the effective global stiffness matrix. The problem is first solved in the transform domain itself, and then an inverse Laplace transformation on the resultant field variables is employed to yield the time-domain solution at desired times of interest. Pertinent details of the approach, computational methodology adopted, convergence studies and accuracy of results are described in detail. Numerical test cases are compared with exact analytic solutions to verify the method. In addition, the practical applicability of the method for scattering and radar cross section prediction for two-dimensional problems is presented for illustration.

keyword: Computational electro magnetics (CEM); Time/frequency domain CEM; Maxwell's equation; Laplace transform; Radar Cross Section (RCS)

1 Introduction

Electromagnetic (EM) field problems permeate several fields of study in electrical engineering from high power machines to high bandwidth communications. Design of electric machinery is critically dependent on accurate solutions of magnetic and electric fields in the stationary and rotating parts of motors and generators. Power electronic designers today are investing more and more resources in calculating and minimizing the electromagnetic interference caused by high power switching circuits. Semiconductor device design is another area where the classical lumped parameter models for circuit elements like resistors, capacitors and inductors are becoming less and less valid as their operating frequencies go higher and higher. Communication systems need constant improvement of signal-to-noise ratio which calls for more exact characterization of the media. Design of antennas and receivers need reasonably accurate EM field solutions. In short, from milli-watt to mega-watt, from 60 hertz to several giga-hertz, Electrical Engineering today leans on accurate methods to obtain solutions for electromagnetic fields.

The similarity of electromagnetic field problems to those in fluid flow have to an extent also inspired the analysis of the former using finite element techniques commonly used for fluid flow computations [Morgan., Hassan, and Peraire (1994); Morgan, Hassan, and Peraire (1996)]. Various methods of analysis exist in the literature from both computational and mathematical viewpoints. To date, of the various approaches existing in the literature, there are two principal schools of thought, namely, time domain analysis and frequency domain analysis. However, EM fields, for the most part, are linear, and so simpler methods can give equally accurate yet effective advantages in the computations of the resulting solutions with improved efficiency. For example, yet effective, transforming the field variables to the transform domain eliminates the time dimension and en-

---

[1] Doctoral student, philip@ece.umn.edu, Department of Electrical and Computer Engineering, EE/CSci 4-178, 200 Union Street S.E. University of Minnesota, MN 55455

[2] Research associate, Department of Mechanical Engineering, AHPCRC, University of Minnesota, MN, U.S.A., ramdev@me.umn.edu, Ph: 612-626-8101, Fax: 612-626-1596.

[3] Professor, and Technical Director, Department of Mechanical Engineering, and AHPCRC, University of Minnesota, MN, U.S.A. ktamma@tc.umn.edu, Ph: 612-626-8102, Fax: 612-626-1596.

ables the problem to be considered as a quasi-steady-state one. No restricted time-stepping is necessary - a straight forward inverse transformation of the Laplace transform solution can give the solution at any desired time instant. Laplace transform techniques have been used for the analysis of linear transient and a class of non-linear transient problems in heat conduction [Tamma and Railkar (1988a),Tamma and Railkar (1988b)] and structural dynamics [Yao, Fung, and Tseng (1999)] and [Beskos and Boley (1975)]. Along similar lines, Cai and Costache [Cai and Costache (1994)] describe a method to decompose the system to individual modes by eigen value decomposition. The inverse Laplace transform of the resultant modal equations is straightforward, which gives the time domain solution at any instant. However, this method is not practical for large problems because of the requirement of eigen value decomposition. For related hybrid methods in frequency domain refer to [Reddy (2004)].

In contrast, in this study, the numerical inversion of the Laplace transform is performed using the method developed by Durbin [Durbin (1974)]. Time scaling of Maxwell's equations is proposed to improve the conditioning of the element and global matrices (this technique also applies to time-domain methods as well). Further, decoupling of the Maxwell's EM equations into two groups can result in reduction of the global matrix size for planar problems.

A brief introduction to Maxwell's equations is given in Section 2. Section 2.3 describes the benefits of time-scaling of Maxwell's equations which can improve the condition of the finite element matrices. Section 2.4 explains how two decoupled systems of equations can be formed for planar electromagnetic problems. The weak formulation of the problem using Galerkin's method is detailed in Section 3, and the inversion procedure for the Laplace transform domain solution is explained in Section 4. Some novel and interesting issues on the unique, yet effective strategies via the present developments for subsequent use in large-scale computations are highlighted with particular attention to contrasting the difference with the traditional paradigms for solving time domain and the so-called frequency domain computational electro magnetic (CEM) equations. Numerical examples to verifying the present developments are given in Section 5. The remaining two sections contain discussions highlighting the pros/cons and the relevant conclu-
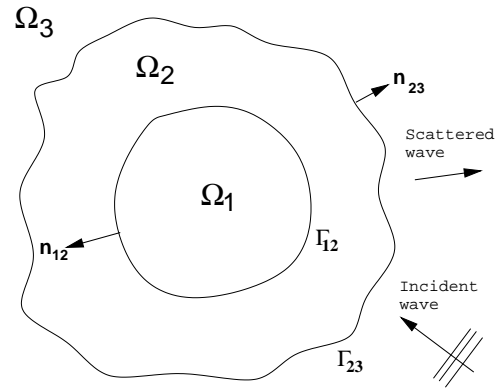
Figure 1 : Problem description, domain, boundaries and boundary conditions.

sions and future directions.

2 Maxwell's Equations

2.1 *Maxwell's equations in time domain*

The behavior of electric and magnetic fields, with and without the presence of a medium, are completely determined by a set of partial differential equations known as the Maxwell's equations. In their most general sense, they can be written in non-integral form as [Wangsness (1979)]

$$\nabla \times \mathbf{E} = -\frac{\partial \mathbf{B}}{\partial t} \tag{1}$$

$$\nabla \times \mathbf{H} = \mathbf{J} + \frac{\partial \mathbf{D}}{\partial t} \tag{2}$$

$$\nabla \cdot \mathbf{D} = \rho_f \tag{3}$$

$$\nabla \cdot \mathbf{B} = 0 \tag{4}$$

where $\mathbf{E}$ is the electric field, $\mathbf{H}$ is the magnetic field, $\mathbf{D}$ is the electric flux density, $\mathbf{B}$ is the magnetic flux density, $\mathbf{J}$ is the free current density, and ρ_f is the free charge density.

It should be noted that in a charge-free medium ($\rho = 0$), Equation 3 can be derived from Equation 1 and Equation 4 from Equation 2. In addition, these fields have to satisfy the boundary conditions at any interface Γ_{ij} between the two media Ω_i and Ω_j, given by

$$\hat{\mathbf{n}} \cdot (\mathbf{D}_j - \mathbf{D}_i) = \sigma_f \tag{5}$$

$$\hat{\mathbf{n}} \times (\mathbf{E}_j - \mathbf{E}_i) = 0 \tag{6}$$

$$\hat{\mathbf{n}} \cdot (\mathbf{B}_j - \mathbf{B}_i) = 0 \tag{7}$$

$$\hat{\mathbf{n}} \times (\mathbf{H}_j - \mathbf{H}_i) = \mathbf{K}_f \tag{8}$$

where, $\hat{\mathbf{n}}$ is the unit normal to the interface, pointing from region Ω_i to region Ω_j, σ_f is the surface charge density at the interface, and $\mathbf{K}_f$ is the surface current density at the interface. Constitutive properties for a uniform isotropic medium, namely, the electric and the magnetic flux densities and the current density can be completely characterized by

$$\mathbf{D} = \varepsilon\mathbf{E} \tag{9}$$
$$\mathbf{B} = \mu\mathbf{H} \tag{10}$$
$$\mathbf{J} = \sigma\mathbf{E} \tag{11}$$

where, ε is the permittivity, μ is the permeability, and σ is the conductivity of the medium. Employing the Eqs. 9 – 11, Maxwell's equations can be simplified as

$$\nabla \times \mathbf{E} = -\mu\frac{\partial \mathbf{H}}{\partial t} \tag{12}$$
$$\nabla \times \mathbf{H} = \sigma\mathbf{E} + \varepsilon\frac{\partial \mathbf{E}}{\partial t} \tag{13}$$
$$\nabla \cdot \mathbf{E} = 0 \tag{14}$$
$$\nabla \cdot \mathbf{H} = 0 \tag{15}$$

Using Eq. 9 through 11, the boundary conditions to be satisfied by the electric and magnetic fields can be simplified as

$$\hat{\mathbf{n}} \cdot (\varepsilon_i\mathbf{E}_j - \varepsilon_j\mathbf{E}_i) = \sigma_f \tag{16}$$
$$\hat{\mathbf{n}} \times (\mathbf{E}_j - \mathbf{E}_i) = 0 \tag{17}$$
$$\hat{\mathbf{n}} \cdot (\mu_i\mathbf{H}_j - \mu_j\mathbf{H}_i) = 0 \tag{18}$$
$$\hat{\mathbf{n}} \times (\mathbf{H}_j - \mathbf{H}_i) = \mathbf{K}_f \tag{19}$$

Within a perfect conductor, both the electric and magnetic fields are zero. Hence on a conductor surface we have $\mathbf{E}_j = 0$ and $\mathbf{H}_j = 0$ in Eq. 16 through Eq. 19. In this case,

$$\hat{\mathbf{n}} \cdot \mathbf{E}_i = -\frac{\sigma_f}{\varepsilon_i} \tag{20}$$
$$\hat{\mathbf{n}} \times \mathbf{E}_i = 0 \tag{21}$$
$$\hat{\mathbf{n}} \cdot \mathbf{H}_i = 0 \tag{22}$$
$$\hat{\mathbf{n}} \times \mathbf{H}_i = -\mathbf{K}_f \tag{23}$$

In other words, a conductor interface imposes constraints on the tangential component of the electric field, and the normal component of the magnetic field.

For any medium, we define the relative permeability μ_r and relative permittivity ε_r, as

$$\mu = \mu_0\mu_r \tag{24}$$
$$\varepsilon = \varepsilon_0\varepsilon_r \tag{25}$$

where, ε_0 is the permittivity of free space $= 8.85419 \times 10^{-12}$ F/m, and μ_0 is the permeability of free space $= 4\pi \times 10^{-7}$ H/m. Also, the velocity of propagation of an electromagnetic wave in a medium is given by

$$c = \frac{1}{\sqrt{\mu\varepsilon}} \tag{26}$$

The characteristic impedance of the medium is defined as

$$\eta = \sqrt{\frac{\mu}{\varepsilon}} \tag{27}$$

In free space, the quantities c and η become

$$c_0 = \frac{1}{\sqrt{\mu_0\varepsilon_0}}; \quad \eta_0 = \sqrt{\frac{\mu_0}{\varepsilon_0}} \tag{28}$$

2.2 Maxwell's equations in Laplace domain

Using Laplace transforms of $\mathbf{E}$ and $\mathbf{H}$, we can write Eq. 12 through Eq. 15 as

$$\nabla \times \overline{\mathbf{E}} = -\mu(s\overline{\mathbf{H}} - \mathbf{H}_0) \tag{29}$$
$$\nabla \times \overline{\mathbf{H}} = (\sigma + \varepsilon s)\overline{\mathbf{E}} - \varepsilon\mathbf{E}_0 \tag{30}$$
$$\nabla \cdot \overline{\mathbf{E}} = 0 \tag{31}$$
$$\nabla \cdot \overline{\mathbf{H}} = 0 \tag{32}$$

where $\overline{\mathbf{E}}$ and $\overline{\mathbf{H}}$ are Laplace transforms of $\mathbf{E}$ and $\mathbf{H}$ respectively, and $\mathbf{E}_0$ and $\mathbf{H}_0$ are the initial values.

2.3 Time Scaling of Maxwell's Equations

The differential equations which govern the electric and magnetic fields have been discussed in the previous section. The numerical values of μ and ε are very low, and can cause the effective element and global stiffness matrices to be ill-conditioned because of very small diagonal entries. To overcome this problem, we apply a time scaling by c_0, i.e., we define $\tilde{t} = c_0 t$. Hence, the complex frequency variable s gets scaled as $\tilde{s} = \frac{s}{c_0}$ Thus, we can rewrite Eq. 29 through 32 as

$$\nabla \times \overline{\mathbf{E}} = -\mu c_0(\tilde{s}\overline{\mathbf{H}} - \mathbf{H}_0) \tag{33}$$
$$\nabla \times \overline{\mathbf{H}} = (\sigma + \varepsilon\tilde{s}c_0)\overline{\mathbf{E}} - c_0\varepsilon\mathbf{E}_0 \tag{34}$$
$$\nabla \cdot \overline{\mathbf{E}} = 0 \tag{35}$$
$$\nabla \cdot \overline{\mathbf{H}} = 0 \tag{36}$$

Substituting for c_0 from Eq. 28, we get

$$\nabla \times \sqrt{\epsilon_0}\overline{\mathbf{E}} = -\mu_r\sqrt{\mu_0}(\tilde{s}\overline{\mathbf{H}} - \mathbf{H}_0) \tag{37}$$

$$\nabla \times \sqrt{\mu_0}\overline{\mathbf{H}} = (\sigma\eta_0 + \epsilon_r\tilde{s})\sqrt{\epsilon_0}\overline{\mathbf{E}} - \epsilon_r\sqrt{\epsilon_0}\mathbf{E}_0 \tag{38}$$

$$\nabla \cdot \overline{\mathbf{E}} = 0 \tag{39}$$

$$\nabla \cdot \overline{\mathbf{H}} = 0 \tag{40}$$

We define quantities $\boldsymbol{E}$ and $\boldsymbol{H}$ such that

$$\boldsymbol{E} = \sqrt{\epsilon_0}\mathbf{E} \tag{41}$$

$$\boldsymbol{H} = \sqrt{\mu_0}\mathbf{H} \tag{42}$$

which yields,

$$\nabla \times \overline{\boldsymbol{E}} = -\mu_r(\tilde{s}\overline{\boldsymbol{H}} - \boldsymbol{H}_0) \tag{43}$$

$$\nabla \times \overline{\boldsymbol{H}} = (\sigma\eta_0 + \epsilon_r\tilde{s})\overline{\boldsymbol{E}} - \epsilon_r\boldsymbol{E}_0 \tag{44}$$

$$\nabla \cdot \overline{\boldsymbol{E}} = 0 \tag{45}$$

$$\nabla \cdot \overline{\boldsymbol{H}} = 0 \tag{46}$$

In most cases, for plane wave propagation, the peak value of the electric and magnetic fields are related to each other by [Wangsness (1979)]

$$\frac{|\mathbf{E}|}{|\mathbf{H}|} = \eta \tag{47}$$

From Eq. 24, 25 and 27, we have

$$\eta = \sqrt{\frac{\mu_r}{\epsilon_r}}\eta_0 = 376\sqrt{\frac{\mu_r}{\epsilon_r}} \quad \text{ohms} \tag{48}$$

This means that the magnitudes of the electric and magnetic fields are different by two orders of magnitude. This is generally the case in most wave-propagation problems. However, from Eq. 41 and 42, we have

$$\frac{|\boldsymbol{E}|}{|\boldsymbol{H}|} = \sqrt{\frac{\mu_r}{\epsilon_r}} \tag{49}$$

The magnitudes of $\boldsymbol{E}$ and $\boldsymbol{H}$ are of the same order, except in the case of a ferromagnetic medium with high μ_r. Hence, the truncation and roundoff errors affect both the fields equally if time-scaling is employed. It is to be noted that this scaling is equally beneficial for time-domain methods as well.

2.4 Decoupling of Maxwell's Equations

In the finite element formulation, for each node of the mesh, we have six degrees of freedom, three each for $\mathbf{E}$ and $\mathbf{H}$ at a node. However, in some special cases, three of the six degrees of freedom are completely decoupled from the other three. This results in a drastic reduction in the complexity of the problem, and can in some cases, eliminate three degrees of freedom. Such a simplification significantly improves the speed of solution of the resulting effective global stiffness matrix. Expanding Eq. 12 through 15 for a two-dimensional domain, we get

$$\begin{vmatrix} \hat{\mathbf{x}} & \hat{\mathbf{y}} & \hat{\mathbf{z}} \\ \frac{\partial}{\partial x} & \frac{\partial}{\partial y} & 0 \\ E_x & E_y & E_z \end{vmatrix} = -\mu\left(\frac{\partial H_x}{\partial t}\hat{\mathbf{x}} + \frac{\partial H_y}{\partial t}\hat{\mathbf{y}} + \frac{\partial H_z}{\partial t}\hat{\mathbf{z}}\right) \tag{50}$$

$$\begin{vmatrix} \hat{\mathbf{x}} & \hat{\mathbf{y}} & \hat{\mathbf{z}} \\ \frac{\partial}{\partial x} & \frac{\partial}{\partial y} & 0 \\ H_x & H_y & H_z \end{vmatrix} = \epsilon\left(\frac{\partial E_x}{\partial t}\hat{\mathbf{x}} + \frac{\partial E_y}{\partial t}\hat{\mathbf{y}} + \frac{\partial E_z}{\partial t}\hat{\mathbf{z}}\right)$$

$$+ \sigma(E_x\hat{\mathbf{x}} + E_y\hat{\mathbf{y}} + E_z\hat{\mathbf{z}}) \tag{51}$$

$$\frac{\partial E_x}{\partial x} + \frac{\partial E_y}{\partial y} = 0 \tag{52}$$

$$\frac{\partial H_x}{\partial x} + \frac{\partial H_y}{\partial y} = 0 \tag{53}$$

Alternatively,

$$\frac{\partial E_y}{\partial x} - \frac{\partial E_x}{\partial y} = -\mu\frac{\partial H_z}{\partial t} \tag{54}$$

$$\frac{\partial E_z}{\partial y} = -\mu\frac{\partial H_x}{\partial t}; \quad -\frac{\partial E_z}{\partial x} = -\mu\frac{\partial H_y}{\partial t} \tag{55}$$

$$\frac{\partial H_y}{\partial x} - \frac{\partial H_x}{\partial y} = -\epsilon\frac{\partial E_z}{\partial t} + \sigma E_z \tag{56}$$

$$\frac{\partial H_z}{\partial y} = \epsilon\frac{\partial E_x}{\partial t} + \sigma E_x; \quad -\frac{\partial H_z}{\partial x} = -\epsilon\frac{\partial E_y}{\partial t} + \sigma E_y \tag{57}$$

$$\frac{\partial H_x}{\partial x} + \frac{\partial H_y}{\partial y} = 0 \tag{58}$$

$$\frac{\partial E_x}{\partial x} + \frac{\partial E_y}{\partial y} = 0 \tag{59}$$

In other words, the group of variables E_x, E_y, and H_z are completely decoupled from the group H_x, H_y, and E_z. Hence for planar problems, it may be sufficient to consider only one of the groups of variables, by properly orienting the coordinate axes.

3 Weak Formulation

To derive the numerical solution for Eq. 43 through 46, we make use of the Galerkin weighted residual formulation for illustration. Other spatial high-order methods can be readily employed.

$$\int_{\Omega} \mathbf{W}_{c,e}(\nabla \times \overline{\boldsymbol{E}} + \mu_r(\tilde{s}\overline{\boldsymbol{H}} - \boldsymbol{H}_0))d\Omega = 0 \quad (60)$$

$$\int_{\Omega} \mathbf{W}_{c,h}(\nabla \times \overline{\boldsymbol{H}} - ((\sigma\eta_0 + \varepsilon_r\tilde{s})\overline{\boldsymbol{E}} - \varepsilon\boldsymbol{E}_0))d\Omega = 0 \quad (61)$$

$$\int_{\Omega} \mathbf{W}_{d,e}(\nabla \cdot \overline{\boldsymbol{E}})d\Omega = 0 \quad (62)$$

$$\int_{\Omega} \mathbf{W}_{d,h}(\nabla \cdot \overline{\boldsymbol{H}})d\Omega = 0 \quad (63)$$

Choosing the weighting functions to be same as the shape functions, we have

$$\begin{aligned} \mathbf{W}_{c,e} &= \mathbf{N}_e^T; \quad \mathbf{W}_{d,e} = \mathbf{N}_e^T \\ \mathbf{W}_{c,h} &= \mathbf{N}_h^T; \quad \mathbf{W}_{d,h} = \mathbf{N}_h^T \end{aligned} \quad (64)$$

and using the vector identities

$$\begin{aligned} \nabla \times (W\mathbf{A}) &= \nabla W \times \mathbf{A} + W\nabla \times \mathbf{A} \\ \int_{\Omega} \nabla \times \mathbf{A}d\Omega &= \int_{\Gamma} \hat{\mathbf{n}} \times \mathbf{A}d\Gamma \end{aligned} \quad (65)$$

Employing the above identities in Eqns. 60 and 61 yields

$$\begin{aligned} &\mu_r\tilde{s}\int_{\Omega}(\mathbf{W}_{c,e}\overline{\boldsymbol{H}})d\Omega - \int_{\Omega}(\nabla\mathbf{W}_{c,e}\times\overline{\boldsymbol{E}})d\Omega \\ &= \mu_r\int_{\Omega}(\mathbf{W}_{c,e}\boldsymbol{H}_0)d\Gamma - \int_{\Gamma}(\hat{\mathbf{n}}\times\mathbf{W}_{c,e}\overline{\boldsymbol{E}})d\Gamma \quad (66) \end{aligned}$$

$$\begin{aligned} &\mu_r\tilde{s}\int_{\Omega}(\mathbf{W}_{c,h}\overline{\boldsymbol{E}})d\Omega + \int_{\Omega}(\nabla\mathbf{W}_{c,h}\times\overline{\boldsymbol{H}})d\Omega \\ &= \mu_r\int_{\Omega}(\mathbf{W}_{c,h}\boldsymbol{E}_0)d\Gamma + \int_{\Gamma}(\hat{\mathbf{n}}\times\mathbf{W}_{c,h}\overline{\boldsymbol{H}})d\Gamma \quad (67) \end{aligned}$$

In Cartesian coordinates,

$$\begin{aligned} \overline{\boldsymbol{E}} &= \overline{\boldsymbol{E}}_x\hat{\mathbf{x}} + \overline{\boldsymbol{E}}_y\hat{\mathbf{y}} + \overline{\boldsymbol{E}}_z\hat{\mathbf{z}} \\ \overline{\boldsymbol{H}} &= \overline{\boldsymbol{H}}_x\hat{\mathbf{x}} + \overline{\boldsymbol{H}}_y\hat{\mathbf{y}} + \overline{\boldsymbol{H}}_z\hat{\mathbf{z}} \end{aligned} \quad (68)$$

As an illustration, for a simple triangular mesh, we have the shape function $\mathbf{N}$ defined as

$$\mathbf{N} = [\ a_p + b_p x + c_p y \quad a_q + b_q x + c_q y \quad a_r + b_r x + c_r y\ ] \quad (69)$$

For simplicity we choose $\mathbf{N}_e = \mathbf{N}_h = \mathbf{N}$ in Eqn. 68 which results in

$$\begin{aligned} \overline{\boldsymbol{E}}_x &= \mathbf{N}\vec{E}_x; \quad \overline{\boldsymbol{E}}_y = \mathbf{N}\vec{E}_y; \quad \overline{\boldsymbol{E}}_z = \mathbf{N}\vec{E}_z \\ \overline{\boldsymbol{H}}_x &= \mathbf{N}\vec{H}_x; \quad \overline{\boldsymbol{H}}_y = \mathbf{N}\vec{H}_y; \quad \overline{\boldsymbol{H}}_z = \mathbf{N}\vec{H}_z \end{aligned} \quad (70)$$

where $\vec{E}_x = [\ \overline{\boldsymbol{E}}_{x,p}, \overline{\boldsymbol{E}}_{x,q}, \overline{\boldsymbol{E}}_{x,r}, \dots\ ]^T$ and $p, q, r, \dots$ designating the nodes which form the element. One can readily use high-order elements as well as approaches such as discontinuous Galerkin formulations for the spatial aspects with arbitrary order [Hesthaven and Warburton (2004)]. Substituting $\overline{\boldsymbol{E}}$ and $\overline{\boldsymbol{H}}$ (Eqs. 70) in Eq. 60 through 63 we can readily derive the effective element stiffness matrix. Employing Eqs. 54 – 57 in the transformed domain in the Eqs. 66 – 67 yields

$$(\sigma\eta_0 + \varepsilon_r\tilde{s})\mathbf{M_I}\vec{E}_x - \mathbf{M_y}\vec{H}_z = \varepsilon_r\mathbf{M_I}\vec{E}_{x0} \quad (71)$$

$$(\sigma\eta_0 + \varepsilon_r\tilde{s})\mathbf{M_I}\vec{E}_y + \mathbf{M_x}\vec{H}_z = \varepsilon_r\mathbf{M_I}\vec{E}_{y0} \quad (72)$$

$$-\mathbf{M_y}\vec{E}_x + \mathbf{M_x}\vec{E}_y + \mu_r\tilde{s}\mathbf{M_I}\vec{H}_z = \mu_r\mathbf{M_I}\vec{H}_{z0} \quad (73)$$

$$\mu_r\tilde{s}\mathbf{M_I}\vec{H}_x + \mathbf{M_y}\vec{E}_z = \mu_r\mathbf{M_I}\vec{H}_{x0} \quad (74)$$

$$\mu_r\tilde{s}\mathbf{M_I}\vec{H}_y - \mathbf{M_x}\vec{E}_z = \mu_r\mathbf{M_I}\vec{H}_{y0} \quad (75)$$

$$\mathbf{M_y}\vec{H}_x - \mathbf{M_x}\vec{H}_y + (\sigma\eta_0 + \varepsilon_r\tilde{s})\mathbf{M_I}\vec{E}_z = \varepsilon_r\mathbf{M_I}\vec{E}_{z0} \quad (76)$$

The Eqns. 71 through 76 are used to formulate the element matrices. The global matrix can then be formed by assembling the various element matrices. The solution of the resultant system of equations will give the Laplace domain solution of the electric and magnetic fields for a particular value of $\tilde{s}$. Any of the direct methods like Cholesky or Gaussian elimination can be used for solving the system in the transform domain itself. However, for large systems, iterative solvers with preconditioners can improve the solution speed (including element-by-element [EBE] based techniques). The structure of the global system matrix does not change for each solve. Only the values of some of the entries do change. Also, for smaller variations in *s*, the change in system matrix entries themselves is quite small. Hence, a single preconditioner matrix can be used to solve several of the global stiffness matrices. This saves significant amount of time, since obtaining the preconditioner matrix is often a time-consuming process. In all the examples described in this paper, all the solves have been done using the GMRES algorithm [Saad (2002)], which is adapted to solve a complex variable system that significantly improved the solution speed compared to Gaussian elimination. Once the solution is obtained in the transformed domain, the time domain solution can be directly obtained at any desired instant of time.

4 Inversion of Laplace Domain Solution

In the previous section, we have discussed how to pose the EM field problem in the *s*-domain in a finite-element sense, and its solution procedure. The inverse procedure is described next. The Laplace transform of a function $f(t)$ is defined as

$$F(s) = \int_0^\infty e^{-st} f(t) dt \tag{77}$$

The inverse Laplace transform is then,

$$
\begin{aligned}
f(t) &= \frac{1}{2\pi J} \int_{-\infty}^\infty e^{st} F(s) ds \\
&= \frac{1}{2\pi J} \int_{-\infty}^\infty e^{(a+J\omega t)} F(a+J\omega) J d\omega \\
&= \frac{e^{at}}{2\pi} \int_{-\infty}^\infty e^{J\omega t} F(a+J\omega) d\omega \\
&= \frac{e^{at}}{2\pi} \int_{-\infty}^\infty \Big[\Big(\Re(F(a+J\omega)) \cos \omega t \\
&\quad - \Im(F(a+J\omega)) \sin \omega t \Big) \\
&\quad + J \Big(\Re(F(a+J\omega)) \sin \omega t \\
&\quad + \Im(F(a+J\omega)) \cos \omega t \Big) \Big]
\end{aligned} \tag{78}
$$

Since $f(t)$ is real,

$$
\begin{aligned}
\Re(F(a+J\omega)) &= \Re(F(a-J\omega)) \\
\Im(F(a+J\omega)) &= -\Im(F(a-J\omega))
\end{aligned} \tag{79}
$$

and

$$\int_{-\infty}^\infty \Big(\Re(F(a+J\omega)) \sin \omega t + \Im(F(a+J\omega)) \cos \omega t \Big) d\omega = 0 \tag{80}$$

Thus,

$$
\begin{aligned}
f(t) = \frac{e^{at}}{\pi} \int_0^\infty \Big(& \Re(F(a+J\omega)) \cos \omega t \\
& - \Im(F(a+J\omega)) \sin \omega t \Big) d\omega
\end{aligned} \tag{81}
$$

Also, for causal systems, $f(t) = 0, t < 0$. Hence,

$$
\begin{aligned}
\int_0^\infty \Big(& \Re(F(a+J\omega)) \cos \omega t \\
& + \Im(F(a+J\omega)) \sin \omega t \Big) d\omega = 0
\end{aligned} \tag{82}
$$

In other words,

$$
\begin{aligned}
f(t) &= \frac{2e^{at}}{\pi} \int_0^\infty \Re(F(a+J\omega)) \cos \omega t \, d\omega \\
&= -\frac{2e^{at}}{\pi} \int_0^\infty \Im(F(a+J\omega)) \sin \omega t \, d\omega
\end{aligned} \tag{83}
$$

Using the algorithm described by Durbin [Durbin (1974)], we get

$$
\begin{aligned}
f(t) + \sum_{k=1}^\infty e^{-akT} f(akT+t) &= \frac{2e^{at}}{T} \Big[\frac{1}{2} \Re(F(a)) \\
&+ \sum_{k=1}^{N_{SUM}} \Big(\Re(F(a+\frac{J2\pi k}{T})) \cos \frac{2\pi kt}{T} \\
&- \Im(F(a+\frac{J2\pi k}{T})) \sin \frac{2\pi kt}{T} \Big) \\
&+ \sum_{N_{SUM}+1}^\infty \Big(\Re(F(a+\frac{J2\pi k}{T})) \cos \frac{2\pi kt}{T} \\
&- \Im(F(a+\frac{J2\pi k}{T})) \sin \frac{2\pi kt}{T} \Big) \Big]
\end{aligned} \tag{84}
$$

The second summation on the right side is the truncation error ε_t. The second term on the left side is the error arising due to the algorithm itself, which we refer to as ε_a. Thus,

$$\varepsilon_a = \sum_{k=1}^\infty e^{-akT} f(akT+t) \tag{85}$$

$$
\begin{aligned}
\varepsilon_t = \frac{2e^{at}}{T} \Big[\sum_{N_{SUM}+1}^\infty \Big(& \Re(F(a+\frac{J2\pi k}{T})) \cos \frac{2\pi kt}{T} \\
& - \Im(F(a+\frac{J2\pi k}{T})) \sin \frac{2\pi kt}{T} \Big) \Big]
\end{aligned} \tag{86}
$$

Then, Eq. 84 becomes,

$$
\begin{aligned}
f(t) + \varepsilon_a &= \frac{2e^{at}}{T} \Big[\frac{1}{2} \Re(F(a)) \\
&+ \sum_{k=1}^{N_{SUM}} \Big(\Re(F(a+\frac{J2\pi k}{T})) \cos \frac{2\pi kt}{T} \\
&- \Im(F(a+\frac{J2\pi k}{T})) \sin \frac{2\pi kt}{T} \Big) \Big] + \varepsilon_t
\end{aligned} \tag{87}
$$

5 Illustrative Examples

To verify the overall formulations, a few simple wave propagation problems are solved and compared with analytical results. Detailed analysis of these test cases can be found in [Ramo, Whinnery, and Duzer (1979)] and [Harrington (1961)].
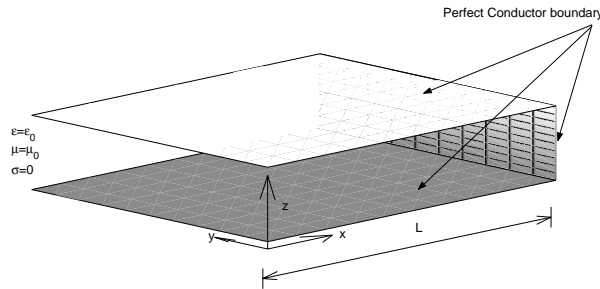
Figure 2 : Transmission line analyzed in numerical examples 1 and 2.

5.1 Plane wave along a transmission line with electric field along y-direction

A plane electromagnetic (Transverse Electric and Magnetic) wave is incident on a lossless transmission line whose major dimension is along the x-direction (see Fig. 2). The initial value of the fields are given by

$$E_{y0} = 0; \quad E_{z0} = e^{-(\frac{x-x_0}{b})^2}$$
$$H_{y0} = \frac{1}{\eta_0}e^{-(\frac{x-x_0}{b})^2}; \quad H_{z0} = 0 \tag{88}$$

The boundary conditions are $E_y = 0$ for $x = 0$, $x = L$ where L is the length of the line.

5.1.1 Analytical solution

For a plane wave propagating in x-direction,

$$E_x = H_x = 0 \tag{89}$$

Also, since $E_{y0} = 0$ and $H_{z0} = 0$, we have

$$E_y = H_z = 0 \text{ for } t \geq 0 \tag{90}$$

For a lossless transmission line, $\sigma = 0$. Then, from equations 54 through 57, we get

$$\frac{\partial E_z}{\partial x} = \mu\frac{\partial H_y}{\partial t}$$
$$\frac{\partial H_y}{\partial x} = \varepsilon\frac{\partial E_z}{\partial t} \tag{91}$$

Thus,

$$\frac{\partial^2 E_z}{\partial x^2} = \mu\varepsilon\frac{\partial^2 E_z}{\partial t^2} \tag{92}$$

The analytical solution for the above problem is given as

$$E_z(x,t) = A_0\sum_{n=1}^{\infty}e^{-(\frac{n\pi b}{2L})^2}\sin(\omega t + \omega_0)\sin\frac{n\pi x}{L}$$
$$H_y(x,t) = -A_0\sum_{n=1}^{\infty}e^{-(\frac{n\pi b}{2L})^2}\cos(\omega t + \omega_0)(1 - \cos\frac{n\pi x}{L}) \tag{93}$$

where $A_0 = \frac{2b\sqrt{\pi}}{L}$ and $\omega_0 = \frac{n\pi x_0}{L}$.

5.1.2 Numerical solution

Given the specification of the problem, we use the variable group H_x, H_y, E_z. Then, from equations 71 through 76, we form the element matrix as

$$\begin{bmatrix} \mu_r\tilde{s}\mathbf{M_I} & 0 & \mathbf{M_y} \\ 0 & \mu_r\tilde{s}\mathbf{M_I} & -\mathbf{M_x} \\ \mathbf{M_y} & -\mathbf{M_x} & (\sigma\eta_0 + \varepsilon_r\tilde{s})\mathbf{M_I} \end{bmatrix}\begin{bmatrix} \vec{H}_x \\ \vec{H}_y \\ \vec{E}_z \end{bmatrix}$$
$$= \begin{bmatrix} \mu_r\mathbf{M_I}\vec{H}_{x0} \\ \mu_r\mathbf{M_I}\vec{H}_{y0} \\ \varepsilon_r\mathbf{M_I}\vec{E}_{z0} \end{bmatrix} \tag{94}$$

The transmission line parameters were chosen as length=10 m, breadth=0.5 m. A triangular mesh was generated with a resolution of 0.125 m. The incident wave parameters were chosen as $x_0 = 3$ m, $b = 1$ m. Relative permeability μ_r and relative permittivity ε_r were assumed to be unity. For the Laplace transform algorithm, the final time t_f was chosen to be 45 ns. aT was chosen to be 5. Then, $T = \tilde{t}_f = t_fc_0 = 13.5$ m, $a = \frac{5}{13.5} = 0.3704$, N_{SUM} was chosen to be 256. The number of time points at which the solution was sought was taken to be 5, yielding solutions at 9, 18, 27 and 36 ns. A comparison of the computed results with the exact solution is given in Fig. 3.

5.2 Convergence study

To study the effectiveness of the method, several combinations of a and N_{SUM} were tried to solve the same problem. The parameters used are:

- $aT = 0.5$ to 7.5

- $N_{SUM} = 2$ to 1024

- Number of time points $= 64$

- Final time $t_f = 45$ ns
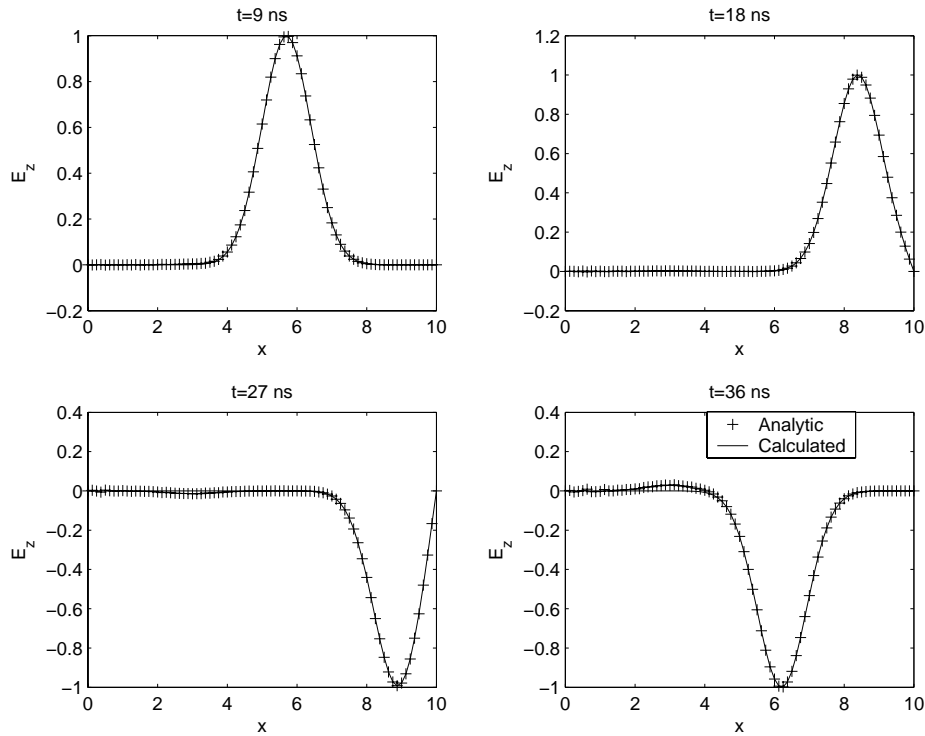
Figure 3 : Time domain solution in comparison with exact solution for plane wave incident on a transmission line, with electric field along z-axis.

The convergence error ε_{conv} is defined as

$$\varepsilon_{conv} = \frac{E^2_{z,numeric} - E^1_{z,numeric}}{max\left(\left|E^1_{z,numeric}\right|\right)} \tag{95}$$

where, $E^1_{z,numeric}$ is the numeric solution of E_z with the current value of N_{SUM} and $E^2_{z,numeric}$ is the numeric solution of E_z with a higher value of N_{SUM}. The absolute error ε_{abs} is

$$\varepsilon_{abs} = \frac{E_{z,numeric} - E_{z,exact}}{max(|E_{z,exact}|)} \tag{96}$$

where $E_{z,exact}$ is the exact analytic solution. The absolute error and convergence error plots thus obtained are shown in Figs. 4 and 5.

From the plots, it is clear that for large values of aT, though there is a potential to achieve better absolute error, convergence is achieved only for large N_{SUM} (Fig. 5b), which is exactly the number of times the global matrix is to be solved. This is due to the fact that the truncation error ε_t is directly related to e^{at} (Eq. 86). When aT is too small, the path of integration gets too close to

the $J\omega$ axis, which gives rise to large errors for a wave propagation problem due to the singularity at $J\omega_0$, where ω_0 is the angular frequency of the wave. In fact, setting $a = 0$ is the same as the Fourier transform method, just as Fourier transform itself is analogous to the Laplace transform with $s = J\omega$. However, the pole on the $J\omega$ axis for wave propagation problems will cause large errors in the Fourier transform method. The present hybrid transform method, however, does not suffer from this problem, and so is well suited for wave propagation problems like the ones discussed in this paper. From Fig. 4, it appears appropriate to choose aT to be around $3.5 - 5$. Another interesting observation is the limit to which the absolute error converges as in Fig. 4a. This is determined by e^{-aT}, as given in [Durbin (1974)]. However large value of N_{SUM} we choose, the absolute error will not be less than ε_a of Eq. 85. As far the convergence plots are concerned, the drawback of large aT is immediately obvious from Fig. 5b where large values of aT, larger N_{SUM} is required for good convergence. As seen in Fig. 5a, the large convergence error (and also absolute error) for small N_{SUM} is partly due to improper frequency sampling which happens at low values of N_{SUM}. In fact, a good
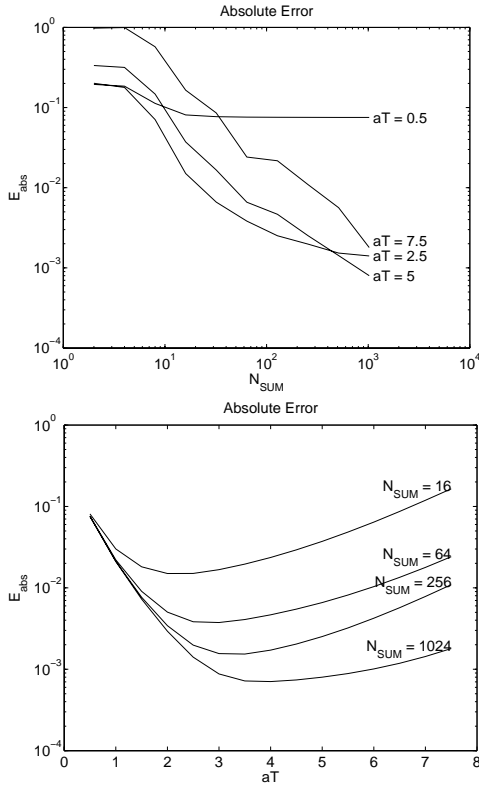
Figure 4 : Convergence of absolute error for different values of N_{SUM} and aT.
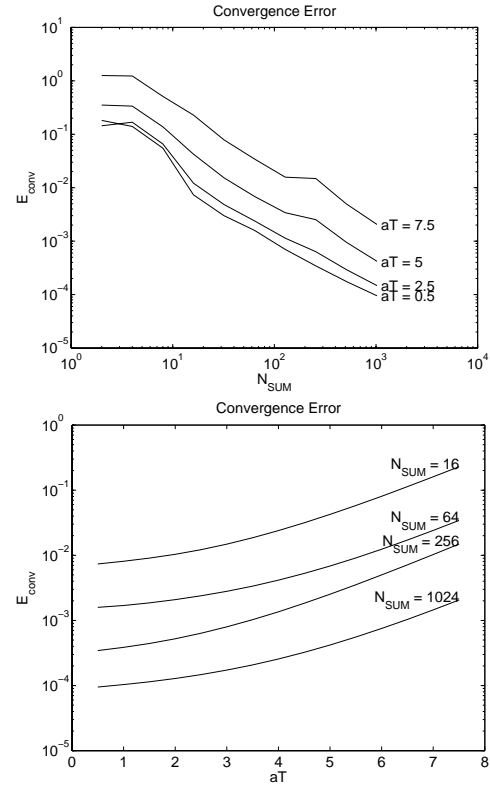
Figure 5 : Convergence of relative error for different values of N_{SUM} and aT.

rule of thumb in choosing N_{SUM} could be the Nyquist criterion of sampling, which states that the sampling frequency should be at least twice the maximum frequency of interest. Using the hybrid transform domain based finite element method, the highest frequency for which the system is solved for is $\frac{N_{SUM}}{t_f}$. Therefore, if the minimum time constant of interest in the system is τ_{min}, then

$$\frac{N_{SUM}}{t_f} > \frac{2}{\tau_{min}} \tag{97}$$

In our example, the significant wavelength of the Gaussian pulse is $\lambda \approx 1.5b$, or 1.5 m. Hence, the significant time period is

$$\tau = \frac{\lambda}{c} = 5 \times 10^{-9} \tag{98}$$

Using the Nyquist criterion, the minimum value of N_{SUM} would be

$$N_{SUM} = \frac{45 \times 10^{-9}}{\frac{1}{2}5 \times 10^{-9}} = 18 \tag{99}$$

However, this is the bare minimum; a good convergence is obtained for N_{SUM} slightly higher than this, normally 3 or 4 times the value obtained by Eq. 97.

6 Scattering Problem and Radar Cross Section (RCS) Computation

Scattering cross section (or Radar cross section) is a measure of the amplitude of a scattered wave from a body in any particular direction. For a plane wave incident on an infinite cylinder, the bistatic scattering cross section per unit length of cylinder, also called the scattering width is given by

$$\sigma(\phi_i, \phi_s) = \lim_{r \to \infty} 2\pi r \frac{|\mathbf{E}_s(r, \phi_s)|^2}{|\mathbf{E}_i(0, \phi_i)|^2} \tag{100}$$

The Radar cross section is then defined as

$$RCS = 10\log(\sigma) \tag{101}$$

6.1 *Computation of RCS using the proposed hybrid formulations*

The computation of RCS using the hybrid formulation proceeds on similar lines as in the case of the time domain finite element methods. The grid used is unstructured and consists of triangular elements. The finite domain is surrounded by perfectly matched layers (PML). The formulation due to [Sacks, Kingsland, Lee, and Lee (1995)] is employed for the purpose as to approximate an infinite domain. Equations 1 were then solved using the present formulations. The finite domain solution is then converted to a far field solution. If $\mathbf{E}_s$ and $\mathbf{H}_s$ are the solutions for the scattered electric and magnetic fields on a surface S, then the corresponding fields at any point $\mathbf{r_0}$ can be obtained using the relation; see Bladel (1985)

$$
\begin{aligned}
\mathbf{E}_s(\mathbf{r_0}) = \frac{1}{4\pi} \int_S &\left[(\hat{\mathbf{n}} \cdot \mathbf{E}_s)\nabla\phi + (\hat{\mathbf{n}} \times \mathbf{E}_s) \times \nabla\phi \right. \\
&\left. - j\omega\mu_0(\hat{\mathbf{n}} \times \mathbf{H}_s)\phi \right] dS \\
\mathbf{H}_s(\mathbf{r_0}) = \frac{1}{4\pi} \int_S &\left[(\hat{\mathbf{n}} \cdot \mathbf{H}_s)\nabla\phi + (\hat{\mathbf{n}} \times \mathbf{H}_s) \times \nabla\phi \right. \\
&\left. - j\omega\varepsilon_0(\hat{\mathbf{n}} \times \mathbf{E}_s)\phi \right] dS
\end{aligned}
\tag{102}
$$

As an example, the scattering of a TE wave by an infinite metal cylinder was analyzed using the proposed developments. The wavelength of the incident wave λ was taken to be same as the radius of the cylinder. The mesh consisted of 15,763 nodes and 30,397 elements, as shown in Fig. 6. aT was chosen to be 5 and $N_{SUM} = 256$. An FFT performed on the steady state solution gave the amplitudes of the scattered wave. Using these values in Eq. 102 gave the far-field quantities. Then, the RCS was computed using Eq. 100 and Eq. 101. The computed RCS was then compared with that calculated using the analytical solution as shown in Fig. 8. The excellent accuracy of the results is noteworthy.

7 Discussion of Hybrid Finite Element Method

The hybrid finite element method with Laplace transforms provides a way of finding the time domain response without time-stepping. For very large meshes, the explicit time stepping approaches often limit the time step due to stability limitations, and other drawbacks such as numerical dispersion are also inherent. Durbin's
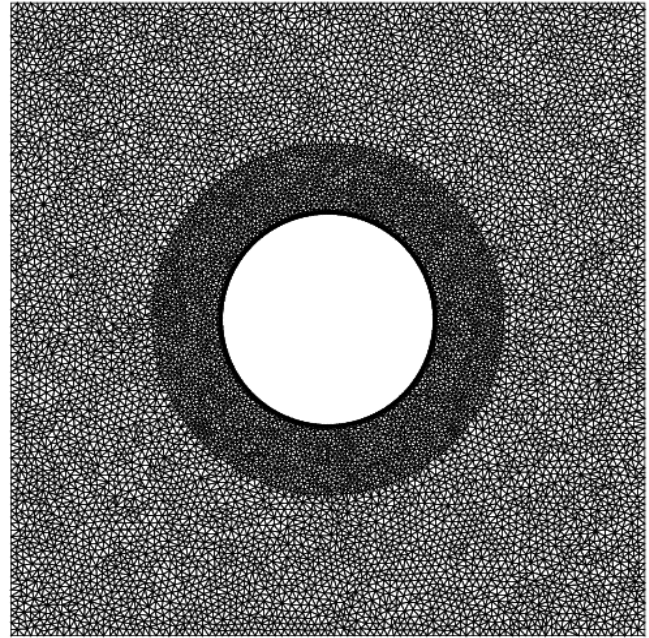
Figure 6 : Scattering of a plane TE wave by a coated perfectly conducting cylinder; Computational domain and the finite element mesh employed.

algorithm approximates the Laplace Inversion to a good extent, but relies on multiple solves of the system for different values of *s*. To have a comparison, let us consider the RCS example considered in the previous section. In the present formulation of the RCS example, we used $N_{SUM} = 256$. The size of the global matrix is given by

$$
N_{g,s} = 2 \times dof \times N_n \tag{103}
$$

where, dof is the degrees of freedom per node and N_n is the number of nodes. For the mesh in the example, $N_n = 15,763$. Hence, $N_{g,s} = 94,578$. Therefore, to find the response at 45 ns, it amounts to 256 solves of the global matrix of size 94,578 (alternatively, an EBE procedure could be readily employed).

For an explicit time-stepping algorithm, the global matrix size is

$$
N_{g,t} = dof \times N_n \tag{104}
$$

In our case, $N_{g,t} = 47,289$. According to [Morgan, Hassan, and Peraire (1996)], the time step required or a time-stepping algorithm is

$$
\Delta t = min(\sqrt{\mu_e\varepsilon_e}h_e) \tag{105}
$$
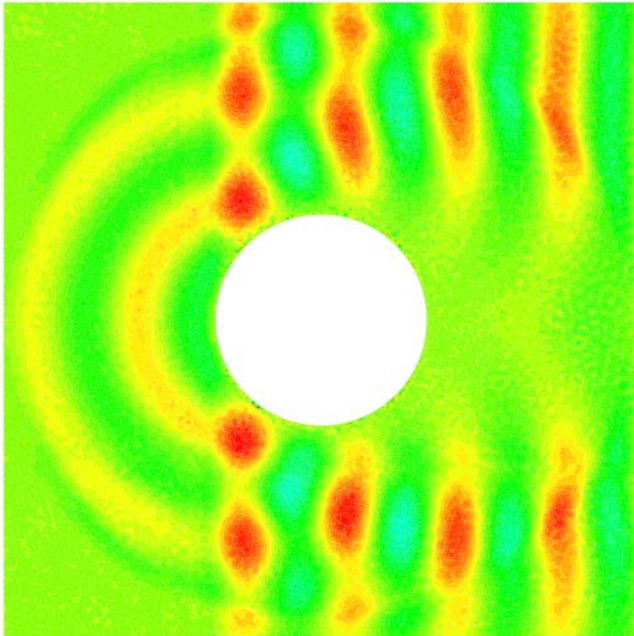
Figure 7 : Scattering of a plane TE wave by a coated perfectly conducting cylinder; Detail of the computed contours of the scattered $\mathbf{E}_z$ field.

Figure 8 : Scattering of a plane TE wave by a coated perfectly conducting cylinder; Comparison between the exact and the computed distribution of the RCS employing the hybrid finite element formulation.

The minimum length of edge in our problem was $h_{e,min} = 0.0078$ m. Thus, $\Delta t = 0.026$ ns. Hence, one needs $\frac{45}{0.026} = 1732$ time step computations with vector operation of size 47,289 to reach 45 ns (and for large transient duration the size is much larger). However, for low-order time stepping methods, the electric and magnetic solutions have significant dispersion error which necessitates the need to employ high-order time stepping methods which increases the effective vector operations by the number of stages employed in the high-order time stepping methods and also the number of time steps employed as the critical time step also reduces with the spatial order of approximations (see Cockburn and Shu (2001) Table 2.2, page 191).

However, for the hybrid method, the real savings comes from the following three facts. First, note that the solve for each s value is independent, and so the formulations can be easily parallelized. For this example, as an illustration, if the analysis is conducted on a 256 processor parallel computer, then effectively there exists the notion of only a single system with a single solve. This is especially attractive for problems analyzed on parallel computers. Much shorter simulation times can be achieved since there is no need of processor communica-

tion during the solve. Second, each of these independent solves can be carefully chosen such that the total number of computation is a minimum. For example, to reduce the numerical error of a solution, we would need double the complex frequency points for which the global matrix is solved, and all the complex frequency points already solved for can be reused. That is, assume that to start with, a problem is analyzed with a minimum number N_{SUM} frequency points. The frequency points used in the analysis are $a, a+J\frac{2\pi}{T}, a+J\frac{4\pi}{T}, a+J\frac{6\pi}{T}, \cdots, a+J\frac{2\pi N_{SUM}}{T}$. To reduce the truncation error by using $2N_{SUM}$ points, we need to solve a global matrix for $a, a+J\frac{2\pi}{T}, a+J\frac{4\pi}{T}, a+J\frac{6\pi}{T}, \cdots, a+J\frac{4\pi N_{SUM}}{T}$. Notice that the solution for the first half of the frequency points are already available and the global matrix needs to be solved only for the complex frequency points higher than $a+J\frac{2\pi N_{SUM}}{T}$. Thus, it is possible to start off at a small N_{SUM} and progressively refine the solution till the desired convergence is achieved. In a typical time-marching methods, to refine the solution, the whole problem would have to be solved again right from the initial state with a smaller time step. Thirdly, the proposed formulations readily permit the solution at any desired time point of interest during a transient analysis without restriction on the step chosen. In this regard, for preliminary design analysis of RCS computations, the approach is fairly effective.

8 Conclusions

A novel hybrid computational methodology for solving Electromagnetic field problems has been developed using the inverse Laplace transform technique of Durbin [Durbin (1974)]. Numerical results were compared with the exact analytical solutions and were found to be of good accuracy. The method promises a number of advantages; in particular over the traditional paradigms of time-stepping methods, and also the frequency domain analysis. The considerations include:

- The global matrix for each complex frequency is independent of the other frequency points; hence, the solution can be easily parallelized on a multi-node super-computer, without any inter-nodal communication.

- In a single-processor scenario, the fact that the variation of the global matrix from one frequency point to a nearby frequency point is usually small obviates the need for preconditioning the global matrix at each step, which can yield significant improvement in solve times.

- The system solution can be refined simply by considering more complex frequency points and adding on to the already obtained solution. There is no need to restart the solve process.

- The method gives good results for the present case of RCS computations in electromagnetic wave-propagation problems since the complex frequency integration contour avoids any poles of the system, including the ones on the $J\omega$ axis.

- The approach has the advantage of obtaining the solution at any desired time point of interest without severe restrictions such as those placed on time stepping based methods.

References

Beskos, D. E.; Boley, B. A. (1975): Use of Dyanmic Influence Coefficients in Forced Vibration Problem with the Aid of Laplace Transform. *Computers & Structures*, vol. 5, pp. 263–269.

Bladel, V. (1985): *Electromagnetic Fields*. Hemisphere Publishing Corporation.

Cai, X.-D.; Costache, G. I. (1994): A Laplace Domain Finite Element Method (LDFEM) Applied to Diffusion and Propagation Problems in Electrical Engineering. *International Journal of Numerical Modelling: Electronic Networks, Devices and Fields*, vol. 7, pp. 419–432.

Cockburn, B.; Shu, C.-W. (2001): Runge-Kutta Discontinuous Galerkin Methods for Convection-Dominated Problems. *Journal of Scientific Computing*, vol. 16, pp. 173–261.

Durbin, F. (1974): Numerical Inversion of Laplace Transform: An Efficient Improvement to Durbin and Abate's Method. *Comp. J.*, vol. 17, pp. 371–376.

Harrington, R. F. (1961): *Time Harmonic Electromagnetic Fields*. McGraw-Hill Book Co.

Hesthaven, J. S.; Warburton, T. (2004): High-Order Accurate Methods for Time-domain Electromagnetics. *CMES: Computer Modeling in Engineering & Sciences*, vol. 5, no. 5, pp. 395-408.

Morgan., K.; Hassan, O.; Peraire, J. (1994): An Unstructured Grid Algorithm for the Solution of Maxwell's Equations in the Time Domain. *International Journal for Numerical Methods in Fluids*, vol. 19, pp. 849–863.

Morgan, K.; Hassan, O.; Peraire, J. (1996): A Time Domain Unstructured Grid Approach to the Simulation of Electromagnetic Scattering in Piecewise Homogeneous Media. *Comput. Methods Appl. Mech. Engrg.*, vol. 134, pp. 17–36.

Ramo, S.; Whinnery, J. R.; Duzer, T. V. (1979): *Fields and Waves in Communication Electronics*, volume 3. John Wiley and Sons.

Reddy, J. (2004): The Characteristic Basis Function Method: A New Technique for Fast Solution of Radar Scattering Problem. *CMES: Computer Modeling in Engineering & Sciences*, vol. 5, no. 5, pp. 455-462.

Saad, Y. (2002): *SPARSKIT: A Basic Tool-kit for Sparse Matrix Computations (Version 2.0)*. University of Minnesota, Department of Computer Science and Engineering, 2002.

Sacks, Z. S.; Kingsland, D. M.; Lee, R.; Lee, J.-F. (1995): A Perfectly Matched Anisotropic Absorber for Use as an Absorbing Boundary Condition. *IEEE Transactions on Antennas and Propagation*, vol. 43, pp. 1460–1463.

Tamma, K. K.; Railkar, S. B. (1988): Hybrid Transfinite Element Modelling and Analysis of Non-Linear Heat Conduction Problems Involving Phase Change. *Engineering Computations*, vol. 5, pp. 117–122.

Tamma, K. K.; Railkar, S. B. (1988): On Heat Displacement Based Hybrid Transfinite Element Formulations for Uncoupled/Coupled Thermally Induced Stress Wave Propagation. *Computers & Structures*, vol. 30, pp. 1025–1036.

Wangsness, R. K. (1979): *Electromagnetic Fields*. John Wiley and Sons.

Yao, C.-M.; Fung, R.-F.; Tseng, C.-R. (1999): Nonlinear Vibration Analysis of a Travelling String with Time-dependent Length by New Hybrid Laplace Transform Finite Element Method. *Journal of Sound and Vibration*, vol. 219, no. 2, pp. 323–337.